Research Square

Preprints are preliminary reports that have not undergone peer review.
They should not be considered conclusive, used to inform clinical practice,
or referenced by the media as validated information.

Human second-trimester amniotic fluid as a source of induced mesenchymal stem cells for regenerative applications

Michelangelo Corcelli

m.corcelli@ucl.ac.uk

University College London

Ellen Petzendorfer

University College London

Kate Hawkins

University College London

Filipa Vlahova

University College London

Pascale V Guillot

University College London

Article

Keywords: extracellular vesicles, fetal stem cells, mesenchymal stem cells

Posted Date: September 23rd, 2026

DOI: https://doi.org/10.21203/rs.3.rs-10807257/v1

License: This work is licensed under a Creative Commons Attribution 4.0 International License.
Read Full License

Additional Declarations: No competing interests reported.

Abstract

Human fetal mesenchymal stem/stromal cells (hfMSCs) display several advantageous properties compared with their adult counterparts and human amniotic fluid stem cells (AFSCs) have been shown to improve bone extracellular matrix quality and structure. However, the clinical translation of primary hfMSCs remains limited by donor-to-donor variability, limited expansion capacity and replicative senescence, which are associated with progressive loss of tissue-repair potential. To address these limitations, we reprogrammed AFSCs to pluripotency and subsequently directed AFSC-derived hiPSCs towards the mesodermal lineage to generate induced mesenchymal stem/stromal-like cells (AF-iMSCs). AF-iMSCs retained key MSC features, including expression of canonical mesenchymal markers and trilineage differentiation potential. Comparative gene-expression analysis showed that AF-iMSCs expressed higher levels of genes associated with mesenchymal stromal identity, cell signalling, adhesion, migration, extracellular matrix remodelling and osteogenic differentiation, whereas AFSCs expressed higher levels of genes linked to proliferative and growth-factor signalling. In addition, AF-iMSCs secreted small extracellular vesicles (iEVs) that promoted fibroblast migration and supported type I collagen and elastin production in vitro, indicating functional pro-reparative activity. Together, these findings suggest that iPSC-mediated derivation of AF-iMSCs provides a scalable and reproducible strategy to overcome key limitations of primary AFSCs and support the development of cell-based and extracellular vesicle-based regenerative therapies.

Introduction

Human mesenchymal stem cells (MSCs) have emerged as a promising tool in regenerative medicine due to their multipotent differentiation capacity, immunomodulatory properties, and ability to promote tissue repair. Their ability to differentiate into mesodermal lineages, including osteocytes, chondrocytes, and adipocytes, make them valuable candidates for bone regeneration, cartilage repair, and other clinical applications. While adult MSCs derived from bone marrow, adipose tissue, and other sources have been extensively studied, fetal mesenchymal stem/stromal cells (hfMSCs) isolated during pregnancy from various fetal tissues[1], placenta[2] and amniotic fluid[3, 4] have long attracted interest due to their enhanced proliferative capacity, superior differentiation potential, and reduced immunogenicity compared to their adult counterparts.[5–7] They also exhibit higher telomerase activity, longer telomeres, and increased plasticity, allowing for more robust expansion in vitro.[7] These characteristics make hfMSCs attractive for therapeutic applications and their regenerative potential has been reported in various preclinical models, including Alport disease[8], brittle bone disease[9–13] and neonatal encephalopathy[14] and in several clinical trials.[15],[16]

Human mid-trimester amniotic fluid, obtained by amniocentesis during ongoing pregnancy, represents a well-established source of highly potent fetal stem cells, commonly refered to as amniotic fluid stem cells (AFSCs)[3, 17], with applications in cell therapy, tissue engineering and disease modelling.[3, 4] AFSCs are easy to reprogram to pluripotency and were shown to be receptive to chemically-induced reprogramming using small molecule epigenetic modifiers.[18–20] They have also emerged as an

effective therapeutic cell source for skeletal regenerative applications.[21, 22] When transplanted perinatally into an experimental model of severe osteogenesis imperfecta, AFSCs reduced bone fragility by decreasing fracture susceptibility, increasing bone strength, improving bone quality and micro-architecture, normalising bone remodelling, and promoting endogenous osteogenesis and maturation of resident osteoblasts.[13]

However, several challenges remain before primary AFSCs can be routinely translated into clinical use. First, their therapeutic efficacy is donor-dependent, resulting in donor-to-donor variability and potentially non-standardised clinical outcomes. [1, 6, 23] Additional challenges include the lack of robust protocols for generating standardized cell preparations, as well as concerns regarding safety, ectopic engraftment or differentiation, immunological rejection, and ethical concerns. Finally, obtaining a sufficient number of donor cells typically requires extensive *in vitro* expansion. However, as primary AFSCs undergo repeated divisions *in vitro*, they eventually enter a state of replicative senescence, characterised by a progressive loss of proliferative capacity.[24] This restricts the scalable expansion cells and may limit the generation of sufficient cell numbers for clinical applications, particularly in settings requiring high-dose or repetitive-dose administration.[24] In addition, senescent stem cells exhibit reduced differentiation potential across key mesenchymal lineages, and may show impaired paracrine efficacy, thereby limiting their ability to modulate and normalise target cell behaviour. Senescence also reduces the capacity of stem cells to home to injury sites and engraft within tissues, compromising their ability to support tissue repair. This represents a major challenge for standardization, as the repeated identification of new donors is required to generate new stem cell batches, thereby limiting clinical translation and introducing variability in therapeutic intervention outcomes.

To overcome these challenges, human induced pluripotent stem cells (iPSCs) have emerged as a powerful alternative source for the generation of MSCs. Produced by reprogramming somatic cells through the forced expression of key transcription factors, such as OCT4, SOX2, KLF4, and c-MYC, hiPSCs can proliferate indefinitely while retaining the potential to differentiate into lineages of all three germ layers. Importantly, iPSCs can be directed to generate MSC-like cells, commonly referred to as induced MSCs (iMSCs), which share key phenotypic and functional properties with primary MSCs. This approach provides a potentially unlimited source of patient-specific or allogeneic MSC-like cells, thereby reducing donor-dependent variability and overcoming limitations associated with replicative senescence. [25–28] This cost-effective strategy enables the consistent and reproducible manufacture of iMSCs at commercial scale, while maintaining their therapeutic potential and eliminating the need for repeated donors.

In this study, we reprogrammed human mid-trimester AFSCs into hiPSCs and established a directed differentiation strategy to generate AFSC-derived induced MSC-like cells (AF-iMSCs). We show that AF-iMSCs acquire key mesenchymal features, including spindle-shaped morphology, stable proliferative capacity, expression of canonical MSC markers, loss of pluripotency marker expression, and multilineage differentiation potential. We further demonstrate that AF-iMSCs express a broad repertoire of extracellular matrix-associated genes upon osteogenic differentiation and release extracellular

vesicles (iEVs) with pro-reparative activity, supporting cell migration and restoring matrix-associated defects in vitro. Together, these findings identify AF-iMSCs and their extracellular vesicles as a scalable platform with potential relevance for regenerative and skeletal therapeutic applications. Ultimately, this approach may help address current limitations in MSC-based therapies and support the development of more effective and scalable cell-based interventions.

Results

Mesodermal differentiation of human AFSC-derived hiPSCs into AF-iMSCs

To differentiate AF-iMSCs, human iPSCs derived from mid-trimester amniotic fluid stem cells (hAF-iPSCs) were initially plated on Geltrex matrix in essential 8 medium, which is a chemically-defined serum-free, xeno-free cell culture medium that supports long-term pluripotency. AF-iPSCs formed distinct clusters of colonies (Fig. 1A) which expressed markers associated with pluripotency such as live TRA-1-60 (Fig. 1B), Nanog, OCT4A, SOX2, and KLF4 (Fig. 1C). The cells were subsequently detached and replated as single cells on Geltrex matrix in essential 8 medium, with the medium being replaced by mesoderm induction medium the following day, to induce early mesoderm differentiation over a 5-day period (Fig. 1D). The cells were further differentiated down the mesenchymal lineage by replacing the medium with L-glutamine-supplemented mesencult medium, which is animal component-free (ACF), serum-free and extracellular vesicle (EV)-free, and plated on attachment substrate-coated plates. The cells were passaged at 70% confluency and a 1 to 3 ratio for 3 weeks, upon which they displayed a typical mesenchymal morphology, characterised by adherent, spindle-shaped, fibroblast-like cells growing as a dispersed monolayer rather than as compact colonies (Fig. 2A).

Growth kinetic analysis over three weeks showed that AF-iMSCs maintained a stable proliferative profile, with an average population-doubling time of 40 ± 2 h (mean ± SD, $P < 0.05$) (Fig. 2B). The cells lost OCT4A expression and acquired a mesenchymal phenotype, characterised by vimentin expression and robust expression of the canonical MSC-associated surface markers CD73, CD90 and CD105, with 90% cells co-expressing these markers CD73, CD90 and CD105, as assessed by immunofluorescence and flow cytometry (Fig. 2C, D **and E**). Consistent with a mesenchymal phenotype, AF-iMSC were negative for the hematopoietic markers CD34 and CD45 (Fig. 2D).

Transcriptomic analysis reveals significant differences between AF-iMSCs and AFSCs

We used an RT² Profiler™ PCR Array Human Mesenchymal Stem Cells (QIAGEN) to assess gene expression differences between iMSCs and AFSCs for genes that define stromal identity and their differentiation potential (Fig. 3). Out of the 84 target genes tested in triplicate, 31 genes were differentially expressed, showing at least a two-fold difference in gene expression between both lines.

Compared to AFSCs, AF-iMSCs showed higher expression of 26 genes, i.e. ANPEP (Alanyl (membrane) aminopeptidase), CASP3 (Caspase 3, apoptosis-related cysteine peptidase), CTNNB1 (Catenin (cadherin-associated protein), beta 1, 88kDa), ENG (Endoglin), GDF15 (Growth differentiation factor 15), JAG1 (Jagged 1), KAT2B (K(lysine) acetyltransferase 2B), MCAM (Melanoma cell adhesion molecule), PDGFRB (Platelet-derived growth factor receptor, beta polypeptide), PIGS (Phosphatidylinositol glycan anchor biosynthesis, class S), SLC17A5 (Solute carrier family 17 (anion/sugar transporter), member 5), SMAD4 (SMAD family member 4), TGFB1 (Transforming growth factor, beta 1), TGFB3 (Transforming growth factor, beta 3), VCAM1 (Vascular cell adhesion molecule 1), ALCAM (Activated leukocyte cell adhesion molecule), ANXA5 (Annexin A5), CD44 (CD44 molecule), COL1A1 (Collagen, type I, alpha 1), FGF2 (Fibroblast growth factor 2 (basic)), ITGAV (Integrin, alpha V (, antigen CD51), ITGB1 (Integrin, beta 1), MMP2 (Matrix metallopeptidase 2), NT5E (5'-nucleotidase, ecto, CD73), THY1 (Thy-1 cell surface antigen) and VEGFA (Vascular endothelial growth factor A). A total of 5 genes were expressed at a lower level in iMSCs than in AFSCs, i.e. CSF3 (Colony stimulating factor 3), EGF (epidermal growth factor), INS (insulin), KITLG (KIT ligand), and HAT1 (Histone acetyltransferase 1).

Twenty genes associated with lineage specific lineages were also differentially expressed, with AF-iMSC expressing higher levels of genes associated with the osteogenic lineages, i.e. BGLAP (bone gamma-carboxyglutamate protein/osteocalcin), HDAC1 (histone deacetylase 1), PTK2 (protein tyrosine kinase 2/focal adhesion kinase), RUNX2 (runt-related transcription factor 2), SMAD4 (SMAD family member 4), SMURF1 (SMAD-specific E3 ubiquitin protein ligase 1) and SMURF2 (SMAD-specific E3 ubiquitin protein ligase 2), the adipogenic lineage, i.e. PPARG (peroxisome proliferator-activated receptor gamma) and BMP4 (bone morphogenetic protein 4), chondrogenic lineage, i.e. GDF5 (growth differentiation factor 5), GDF6 (growth differentiation factor 6), KAT2B (lysine acetyltransferase 2B), SOX9 (SRY-box transcription factor 9), TGFB1 (transforming growth factor beta 1), tenogenesis lineage, i.e. GDF15 (growth differentiation factor 15), SMAD4 (SMAD family member 4) and TGFB1 (transforming growth factor beta 1), and myogenic lineage i.e. JAG1 (jagged canonical Notch ligand 1) and NOTCH1 (Notch receptor 1), whilst ACTA2 (actin alpha 2, smooth muscle) was more expressed in AFSCs than in AF-iMSCs (Fig. 4).

AF-iMSC trilineage differentiation potential

AF-iMSCs retained multilineage differentiation potential, as demonstrated by their ability to undergo chondrogenic, adipogenic and osteogenic differentiation, evaluated through Alcian Blue staining of glycosaminoglycan-rich extracellular matrix, Oil Red O staining of intracellular lipid droplets, and Alizarin Red staining of mineralised matrix deposition, respectively (Fig. 5A and 5B).

AF-iMSCs secrete small extracellular vesicles (iEVs) that promote human fibroblast migration in vitro

TEM analysis of extracellular vesicles released by iMSCs into the culture medium (iEVs) revealed a predominantly round cup-shaped morphology with a well-defined lipid bilayer, consistent with the typical appearance of extracellular vesicles under electron microscopy (Fig. 5A). The AF-iEV size range and concentration were determined using Tuneable Resistive Pulse Sensing (TRPS), which measures the

change in electrical resistance as individual particles pass through a nanopore. This enables to provide direct particle size and concentration measurement, unlike nanoparticle tracking analysis (NTA, which estimates size based on particle movement/Brownian motion). Analysis showed an average iEV particle diameter range of 96 ± 27.3 nm (mode 78 nm, maximum 238 nm, minimum 68 nm) and a total particle concentration of 2.76e + 10 particles/ml (Fig. 5B). The expression of the canonical extracellular vesicle-associated tetraspanins CD9, CD63 and CD81 on iEVs was assessed by nano-flow cytometry (NanoFCM) (Fig. 5C). Fibroblast cell uptake assay revealed that iEVs are taken up into target fibroblast cell body to deliver their cargo intracellularly (Fig. 6D).

iEV stimulate human fibroblast migration and production of production of type I collagen and elastin in vitro

An *in vitro* cell-exclusion migration assay was performed to determine whether iEVs enhance human fibroblast migration, as a functional measurement of of iEV bioactivity. Treatment of human fibroblasts cultures with iEVs significantly promoted fibroblast migration, as shown by accelerated closure of the cell-free area over 96 h (Fig. 7A). A significant effect was already evident after 24h, when iEV-treated cultures showed a 17.86% reduction in the cell-free area compared with baseline, whereas untreated fibroblasts showed no measurable gap closure (23.0 ± 1.0 vs. 28.0 ± 0.3, mean ± sem, $P < 0.05$). At 48h, 72h and 96h, untreated fibroblasts achieved 21.43%, 42.86% and 92.14% gap closure, respectively, whereas iEV-treated cultures showed markedly enhanced closure of 79.29%, 97.54% and 99.21% gap closure, respectively. Consistently, the remaining cell-free area was significantly smaller in iEV-treated cultures than in untreated controls at each of these time points (5.8 ± 1.7 vs. 22.0 ± 0.6 at 48 h; 0.7 ± 0.1 vs. 16.0 ± 3.2 at 72h; 0.2 ± 0.1 vs. 2.2 ± 0.3 at 96 h; $P < 0.01$for all comparisons) (Fig. 7B).

To assess the functional activity of iEVs in an extracellular matrix-deficient context, human fibroblasts were cultured in the presence of SB431542, a TGF-β receptor inhibitor. SB431542 treatment reduced elastin and type I collagen deposition, as shown by immunofluorescence staining, and decreased soluble type I collagen levels measured by ELISA (1424.0 ± 12.7 in untreated fibroblasts vs. 1224.0 ± 14.0 in SB431542-treated fibroblasts). Notably, addition of iEVs to SB431542-treated fibroblasts restored type I collagen production to levels comparable with untreated controls (1435.0 ± 7.3, $P < 0.01$), supporting a pro-regenerative effect of iEVs on extracellular matrix production (Fig. 8A and 8B).

Discussion

In this study, we generated mesenchymal stem cell-like cells, referred to as AF-iMSCs, from hiPSCs previously reprogrammed from mid-trimester amniotic fluid [29]. Characterisation of AF-iMSCs showed that the cells acquired a typical adherent, spindle-shaped, fibroblast-like morphology, and displayed a mesenchymal immunophenotype, with more than 90% of cells expressing the canonical MSC-associated markers CD73, CD90 and CD105, together with absence of detectable CD45 and CD34 expression. AF-iMSC also retained multilineage differentiation potential, as demonstrated by their ability to undergo osteogenic, adipogenic and chondrogenic differentiation under appropriate induction conditions. In

addition, growth-kinetic analysis showed that AF-iMSCs maintained a stable proliferation rate over four weeks in culture, with an average population-doubling time of approximately 41 hours[30].

Compared with primary AF cells, AF-iMSCs showed increased expression of genes associated with mesenchymal stromal identity, extracellular matrix interaction, tissue remodelling and paracrine regenerative activity. Higher expression of ENG/CD105, NT5E/CD73 and THY1/CD90, together with CD44 and ALCAM/CD166, supports the acquisition of an MSC-like stromal phenotype, consisten with established criteria used to define MSC and iMSC-like populations. [31–33] Upregulation of the perivascular-associated markers MCAM/CD146 and PDGFRB may further indicate acquisition of a pericyte-like stromal programme, a phenotype linked to tissue repair and vascular support.[34, 35] Increased expression of adhesion and matrix-interaction molecules, including ALCAM, VCAM1, CD44, ITGAV and ITGB1, may enhance cell–cell and cell–matrix interactions, migratory capacity and responsiveness to the extracellular microenvironment.[36–39] In parallel, higher COL1A1, MMP2 and ANPEP/CD13 expression suggests an enhanced capacity for extracellular matrix deposition, remodelling and pericellular proteolytic activity, processes that may support matrix repair and tissue integration.[40–43] The concomitant enrichment of trophic, angiogenic and developmental signalling mediators, including FGF2, VEGFA, GDF15, JAG1, TGFB1 and TGFB3, together with the signalling regulators CTNNB1 and SMAD4 and the chromatin-modifying enzyme KAT2B, may further support pro-reparative, pro-angiogenic and lineage-regulatory functions.[44–50] Finally, increased expression of ANXA5, PIGS and SLC17A5 may reflect enhanced membrane organisation, cell-surface protein regulation and vesicle-associated activity, whereas CASP3 expression may indicate preserved regulation of cell turnover and differentiation-associated remodelling rather than simply increased apoptosis.[51–53]

Conversely, AF-iMSCs showed reduced expression of CSF3, EGF, INS, KITLG and HAT1 compared with primary AF cells. Although these differences require functional validation, this transcriptional profile may be advantageous by suggesting a more restricted stromal programme, with reduced inflammatory, haematopoietic/endocrine and excessive mitogenic signalling. Lower CSF3 expression may limit granulopoietic and neutrophil-associated inflammatory cues[54], while reduced KITLG expression may decrease c-KIT-dependent support of haematopoietic progenitors and mast-cell survival or expansion.[55] Similarly, lower expression of EGF and INS may reduce autocrine growth-factor and metabolic signalling, potentially limiting unwanted epithelial, endocrine or adipogenic bias and avoiding excessive proliferative stimulation.[56, 57] Finally, decreased HAT1 expression may reflect reduced replication-associated chromatin acetylation and proliferative stress, which could be beneficial for maintaining a stable MSC-like phenotype.[58, 59] Together, the lower expression of these genes may contribute to an AF-iMSC profile that is less inflammatory, less haematopoietic/endocrine-biased and more compatible with controlled stromal cell-based regenerative applications.

The higher expression of lineage-associated genes in undifferentiated AF-iMSCs compared with primary AF cells suggests that these cells maintain an MSC-like stem/stromal phenotype while exhibiting increased transcriptional readiness to respond to multilineage mesenchymal differentiation signals. Increased expression of osteogenic-associated genes, including RUNX2, BGLAP, PTK2 and KAT2B, may

indicate enhanced readiness to engage bone-forming programmes, as RUNX2 is a central regulator of osteoblast lineage commitment, BGLAP/osteocalcin is associated with osteoblast maturation, PTK2/FAK links extracellular matrix adhesion to osteogenic mechanotransduction, and KAT2B/PCAF has been implicated in BMP-dependent osteogenic differentiation.[50, 60, 61] In parallel, higher expression of BMP4 and PPARG may reflect broader mesenchymal plasticity and responsiveness to adipogenic/osteogenic lineage cues.[62] The concomitant upregulation of GDF5, GDF6, SOX9, TGFB1 and SMAD4 further supports chondrogenic and matrix-regulatory competence, consistent with the established roles of SOX9 and TGF-β/BMP signalling in cartilage lineage specification and extracellular matrix production.[49, 63, 64] Increased expression of SMURF1 and SMURF2 may provide an additional regulatory layer by modulating TGF-β/BMP pathway intensity, potentially preventing excessive or premature signalling activation while maintaining responsiveness to differentiation cues.[65] Finally, higher expression of GDF15, JAG1 and NOTCH1 may indicate acquisition of regenerative, stress-adaptive and Notch-responsive stromal features, which could support tissue repair, cell–cell communication and myogenic/tenogenic lineage responsiveness.[46, 47] Overall, this transcriptional profile suggests that AF-iMSCs may represent a more developmentally competent MSC-like population, transcriptionally poised for multilineage differentiation and regenerative activity.

As many of the regenerative effects of MSCs are mediated through paracrine mechanisms, including the release of extracellular vesicles (EVs), we next investigated whether AF-iMSCs secrete bioactive iEVs capable of modulating key cellular processes involved in tissue repair. AF-iMSCs released iEVs with an average diameter of approximately 96 nm, consistent with the expected size range of small EVs. Functional assays showed that AF-iMSC-derived iEVs enhanced human fibroblast migration and supported extracellular matrix production *in vitro*, including type I collagen and elastin deposition. This is relevant because fibroblast recruitment and extracellular matrix remodelling are essential steps in wound closure and tissue restoration. Thus, these data suggest that AF-iMSC-derived iEVs are not only phenotypically consistent with extracellular vesicles, but also biologically active, and may contribute to the regenerative potential of AF-iMSCs through paracrine regulation of stromal cell behaviour.

In conclusion, the derivation of iMSCs from AFSC-derived iPSCs provides a strategy to address key limitations associated with primary AFSCs, including donor-to-donor variability, limited expansion capacity and replicative senescence, which can restrict scalability and reproducibility for clinical applications. By combining the proliferative potential of hiPSCs with directed mesenchymal differentiation, this approach enables the generation of a more standardised and expandable MSC-like cell population while retaining relevant stromal, multilineage and pro-reparative properties. These findings support AF-iMSCs as a robust and reproducible platform for regenerative applications and suggest that iPSC-mediated reprogramming may help reset or stabilise donor-specific cellular features that otherwise limit the therapeutic use of primary AFSCs.

Methods

Cell culture

Human mid-trimester amniotic fluid mesenchymal stem cells (AFSCs) (passage 7–10), were isolated from the amniotic fluid of a healthy pregnancy at 12 weeks of gestation, which was obtained under ultrasound guidance and according to the ethical approval given by the Research Ethics Committees of Hammersmith & Queen Charlotte's Hospitals (08/H0714/87) in compliance with national guidelines (Polkinghorne) for the collection of fetal tissue for research, as we previously described.[13] Informed consent was obtained from all subjects and/or legal guardians.

In brief, the cells from three individuals were selected for c-KIT positive expression and expanded on plastic culture dishes without feeders in Dulbecco's modified Eagle's medium (DMEM-HG) (Thermo Fisher) supplemented with 10% fetal bovine serum (Biosera), 2 mM L-glutamine, 50 IU/ml penicillin and 50mg/ml streptomycin (Thermo Fisher), at a density of 10^4 cells/cm^2 at 37° C in a 5% CO_2 incubator.

Human primary dermal fibroblast isolated from neonatal foreskin (PCS-201-010, LGC Standards) were cultivated in Dulbecco's modified Eagle's medium (DMEM-HG) (Thermo Fisher) supplemented with 10% fetal bovine serum (Biosera), 2 mM L-glutamine, 50 IU/ml penicillin and 50mg/ml streptomycin (Thermo Fisher), at a density of 10^4 cells/cm^2 at 37° C in a 5% CO_2 incubator. When indicated, cells were cultivated in expansion medium supplemented with 10 μM SB43152 (Sigma).

Derivation of AF-iMSCs from human AFSCs

AFSC were reprogrammed to pluripotency using non-integrative episomal reprogramming, following the manufacturer's instructions (A15960, Thermo Fisher). In short 500,000 AFSC were dissociated with TrypLE and resuspended in 90 μl electroporation buffer supplemented with 20 μl of hSK, hUL and hOCT4. The cells were electroporated using an electroporator (Neon Transfection System, Thermo Fisher), programme C17 and plated in AFSC expansion medium onto a Geltrex-coated vessel (Thermo Fisher) vessel at 37° C in a 5% CO_2 incubator. Upon reaching confluence the next day, the cells were detached and reseeded onto a Geltrex-coated in in Essential E8 culture medium (both from Stemcell Technologies). Colonies were picked on day 20 using a p200 pipette tip, pooled and reseeded in E8 medium supplemented with ROCK inhibitor (Thermo Fisher).

When reaching 50% confluency, AFSC-derived iPSCs were detached using ReLeSR (Stemcell Technologies) and replated as single cells in Essential E8 culture medium. The following day, the culture medium was replaced by mesoderm induction medium, and replaced every day for the following 4 days, upon which the medium was replaced by L-Glutamine-supplemented mesencult ACF medium (Stemcell Technologies), replaced every 48 hours. On day 10, the cells were detached using TrypLE Express (Thermo Fisher) and reseeded at a density of $5x10^4$ cells/cm^2 on attachment substrate-coated plastic vessels in mesencult medium. Once the cells had reached 70% confluency, they were detached and reseeded at a density of $3x10^4$ cells/cm^2 on attachment substrate-coated plastic vessels in mesencult medium. The cells were cultivated at 37° C in a 5% CO_2 incubator.

In vitro differentiation

Cells were differentiated along the osteoblast lineage for 3 weeks in DMEM-LG supplemented with 10 mM β-glycerophosphate, 0.2 mM ascorbic acid and 10^{-8} M dexamethasone, then fixed in 10% formalin. Cells were differentiated along the adipocyte lineage over 2 weeks in DMEM supplemented with 0.5 mM hydrocortisone, 0.5 mM isobutyl methylxanthine and 60 mM indomethacin, then fixed and stained with oil red O. Cells were differentiated along the chondrocyte lineage over 3 weeks in DMEM-LG supplemented with 0.01 µg/ml TGF-β3, 0.1 µM dexamethasone, 0.17 mM ascorbic acid, 1 mM sodium pyruvate, 0.35 mM L-proline, 1% ITSS, 50 µg/ml Linoleic Acid (all reagents from Merck), then cells were fixed in and stained with alcian blue (2%).

Flow cytometry

The cells were detached, washed in flow buffer (PBS + 3%BSA, Merck) and centrifuged at 5000g for 2 minutes before 10^5 cells were resuspended in the appropriate primary antibody, i.e. CD73-PE, CD90-APC and CD105-FITC (Biolegend) at 1:10 dilution in flow buffer and incubated for 1 hour at 4° C. The cells were then washed again with the FACS buffer and analysed using a Becton Dickinson FACScalibur flow cytometer (BD Biosciences) using Cell Quest Pro and FlowJo software. Negative controls were unstained cells.

Immunofluorescence

The cells were washed in PBS, fixed in 4% paraformaldehyde (PFA, Merck) and permeabilized using TritonX (Merck). The cells were then blocked for 30 minutes with blocking buffer (PBS supplemented with 2% bovine serum albumin and 0.1% Tween) and incubated overnight with primary antibodies at their optimal dilution, i.e. OCT4A (Santa Cruz), KLF4 (Stemgent), SOX2 (Abcam), NANOG (Miltenyi Biotec), TRA-1-60 (Invitrogen), CD90 (Abcam), CD73 (BD Biosciences), CD105 (BD Biosciences), CD34 (Dako Cytomation), CD45 (Dako Cytomation), Type I Collagen Collagen I (Biorad, Cat# 2150-001 - Mouse monoclonal IgG anti human Collagen I used 1:50), elastin (Proteintech, Cat# 15257-1AP - affinity purified rabbit polyclonal IgG anti human ELN used at 1:100) then washed and incubated with secondary antibody (Alexa Flour 488 Goat anti-rabbit IgG, Alexa Flour 488 Goat anti-mouse IgG, all from Abcam 1:500) for 1 hour at room temperature. Cells were then counter-stained with 4’,6-diamidino-2-phenylindole (DAPI) and visualized immediately. Live cell imaging was performed using TRA-1-60 Alexa Fluor 488 conjugated kit, following the manufacturer’s instructions (Thermo Fisher Scientific). Images were collected using a Leica DM 6000 fluorescence microscope (40x PLAN APO objective) and transferred to Adobe Photoshop (Adobe Systems).

Growth kinetics

Growth kinetics were assessed for each cell type (iMSCs and AFSCs) in triplicates at 10^4 cells/cm^2 in 10 cm plates in expansion growth medium. Cells were detached when sub-confluent and counted in trypan

blue to exclude dead cells in a hemocytometer before replating in similar density. The doubling times were calculated via this formula: DT = t/(Log2[y/m]), with DT=doubling time, t=time in culture, y=number of cells at end of culture, m=number of cells at beginning of culture, as described previously.[7]

Gene expression analysis

Primary human AFSCs (P7) and human AF-iMSCs (P7) were seeded at a density of $5x10^4$ cell/cm^2 in 6-well plates and cultured for up to 8 days in Mesencult AFC plus growth medium (Stemcell Technologies). Media changes were performed every 2 days and cells were detached upon reaching 80–90% confluency. Total RNA was extracted from either cell type using TRIzol (Thermo Fisher Scientific), followed by RNA clean-up (RNeasy Qiagen) and cDNA synthesis using RT^2 First Strand Kit (Qiagen, Germany). Gene expression was examined by RT^2 Profiler human PCR arrays (PAHS-082Z, Qiagen) and analysed according to the manufacturer's instructions (n = 3 per group).

Isolation and characterisation of extracellular vesicles (iEVs)

Size exclusion chromatography (SEC) was used to isolate iEVs from the conditioned culture supernatant of iMSCs cultivated without serum. The iMSCs culture supernatant was collected and subjected to differential centrifugation, i.e. 300×G for 10 min, followed by 2000×g for 10 min, and 14,000×g for 30 min. The supernatant was then concentrated to 500–1000 µl using 100 KDa Amicon Ultra centrifugal filter units (Merck) before iEVs isolation. A commercially available size exclusion chromatography (SEC) column qEV original/70 nm (Izon Sciences) was used for the isolation of iEVs by following the standard manufacturer protocol. In brief, the column was prewashed with 17 ml of filtered (0.2 µm Minisart syringe filters) Dulbecco's phosphate-buffered saline (DPBS, Merck Life Science) and 500 µl of the concentrated sample was added to the top of the column filter. After the sample had passed down, 6 ml of DPBS was added immediately on the top of the column filter. The first 2.5 ml were discarded and the 5 following fractions (each 500 µl) were pooled and concentrated using 100 KDa Amicon Ultra 2 ml centrifugal filter units. The size profile and concentration of iEVs were then determined using Tuneable Resistive Pulse Sensing (TRPS), using a 150 nm nanopore calibrated with CPC200 particles (NIST-traceable carboxylated polystyrene, 200 nm), and PBS as electrolyte (Izon Sciences).

Transmission Electron Microscopy (TEM) of iEVs

iEV suspension was deposited on Formvar-carbon-coated 200 mesh copper grids (Agar Scientific, Stansted, UK) and fixed using 2% paraformaldehyde (Merck Life Science, UK) with 1% glutaraldehyde (Polysciences). The vesicles were contrasted in uranyl oxalate and embedded in a mixture of methylcellulose (Merck) and uranyl acetate (Polysciences). Samples of iEVs were then observed using Phillips/FEI CM 120 BioTwin TEM at 120 kV for imaging.

Cellular uptake

iEVs were incubated with BioTracker 655 Red Cytoplasmic Membrane Dye (SCT108- Merck) for 15 min at RT at a dilution of 1:200 before being subjected to two steps of centrifugal filtration of 20 min at 4000g at + 4° C using a 100000kDa MWCO 0.5 ml Amicon ultra centrifugal filter (Merck) to remove any unbound dye. Labelled iEVs were then resuspended in DMEM basal culture medium and administered to fibroblast cells. Cells were visualised after 2 h with fluorescence microscopy using a Zeiss Axio Observer A1 inverted microscope. Negative controls with no dye and positive controls with dye only were also acquired.

I n vitro migration assay

$5x10^4$ human fibroblasts were seeded into each side a removable 2 well culture insert in a µ-Dish 35 mm plate, to create a cell-free gap for migration assays (Ibidi). After removing the insert, iEVs were added to the growth medium (DMEM supplemented with 5% EV-depleted FBS) at a concentration of 10^8 iEVs/ml and the gap was monitored at 0, 24, and 48 h and until complete closure. Phase contrast images were acquired using a Zeiss or Leica inverted microscope using a 5x objective. Gap width and cell-free area were measured using the open-source ImageJ wound healing tool. The assay was used to assess the effects of novel therapeutics like EVs in increasing the migration/proliferation of fibroblasts *in vitro*.

Quantification of pro-collagen I alpha1 (COL1A1)

Concentrations of human pro-collagen I alpha1 in cell culture supernatants were determined using human Pro-Collagen alpha1 DuoSet ELISA (Catalog #DY6220-05, R&D Systems, USA) following the manufacturer's protocol. Prior to assaying, samples were centrifuged at 2000xg for 10 min to remove debris and diluted 1:10 in the recommended reagent diluent (1% BSA in PBS). Recombinant standards and samples were loaded in duplicate onto 96-well microplates pre-coated with the capture antibody. Following sequential incubations with the detection antibody and streptavidin-horseradish peroxidase (HRP), colorimetric signal was developed using tetramethylbenzidine (TMB) substrate and terminated with a sulfuric acid (0.2N) stop solution. Optical density was measured at 450nm on a microplate reader (SpectraMax i3x, Molecular Devices, USA), with wavelength correction at or 570. Concentrations were calculated using a four-parameter logistic (4-PL) curve-fit of the standard curve.

Statistical analysis

Statistical analysis was performed using GraphPad 7.0b. Two-way ANOVAs, followed by Bonferroni’s multiple comparison post-hoc test, were used to obtain p values. $P < 0.05$ was considered significant.

Declarations

Author contributions statement

M.C. and P.V.G. conceived and designed the experiments; M.C., E.P., K.H., F.V. and P.V.G. conducted the experiments and performed the data analysis; P.V.G. wrote the paper; all authors reviewed the

manuscript.

Competing interests

The authors declare that they have no competing interests.

Financial declaration

No funding has been received for this work.

Author Contribution

M.C. and P.V.G. conceived and designed the experiments; M.C., E.P., K.H., F.V. and P.V.G. conducted the experiments and performed the data analysis; P.V.G. wrote the paper; all authors reviewed the manuscript.

Data Availability

All data supporting the findings of this study are available within the paper .

References

1. Abdulrazzak, H., Moschidou, D., Jones, G. & Guillot, P. V. Biological characteristics of stem cells from foetal, cord blood and extraembryonic tissues. *J. R Soc. Interface*. **7** (Suppl 6), S689–706 (2010).
2. Jones, G. N. et al. Ontological differences in first compared to third trimester human fetal placental chorionic stem cells. *PLoS One*. **7**, e43395 (2012).
3. Coppi, P. D. et al. Isolation of amniotic stem cell lines with potential for therapy. *Nat. Biotechnol.* **25**, 100–106 (2007).
4. Loukogeorgakis, S. P. & Coppi, P. D. Concise Review: Amniotic Fluid Stem Cells: The Known, the Unknown, and Potential Regenerative Medicine Applications. *Stem Cells*. **35**, 1663–1673 (2017).
5. Guillot, P. V., O'Donoghue, K. & Kurata, H. Fisk, N. M. Fetal stem cells: betwixt and between. *Semin Reprod. Med.* **24**, 340–347 (2006).
6. Guillot, P. V. et al. Comparative osteogenic transcription profiling of various fetal and adult mesenchymal stem cell sources. *Differentiation* **76**, 946–957 (2008).
7. Guillot, P. V., Gotherstrom, C., Chan, J., Kurata, H. & Fisk, N. M. Human first-trimester fetal MSC express pluripotency markers and grow faster and have longer telomeres than adult MSC. *Stem Cells*. **25**, 646–654 (2007).

8. Moschidou, D. et al. Human Chorionic Stem Cells: Podocyte Differentiation and Potential for the Treatment of Alport Syndrome. *Stem Cells Dev.* **25**, 395–404 (2016).
9. Vanleene, M. et al. Ultra-structural defects cause low bone matrix stiffness despite high mineralization in osteogenesis imperfecta mice. *Bone* **50**, 1317–1323 (2012).
10. Vanleene, M. et al. Transplantation of human fetal blood stem cells in the osteogenesis imperfecta mouse leads to improvement in multiscale tissue properties. *Blood* **117**, 1053–1060 (2011).
11. Jones, G. N. et al. Potential of human fetal chorionic stem cells for the treatment of osteogenesis imperfecta. *Stem Cells Dev.* **23**, 262–276 (2014).
12. Guillot, P. V. et al. Intrauterine transplantation of human fetal mesenchymal stem cells from first-trimester blood repairs bone and reduces fractures in osteogenesis imperfecta mice. *Blood* **111**, 1717–1725 (2008).
13. Ranzoni, A. M. et al. Counteracting bone fragility with human amniotic mesenchymal stem cells. *Sci. Rep.* **6**, 39656 (2016).
14. Corcelli, M. et al. Neuroprotection of the hypoxic-ischemic mouse brain by human CD117(+)CD90(+)CD105(+) amniotic fluid stem cells. *Sci. Rep.* **8**, 2425 (2018).
15. Sagar, R. L. et al. An exploratory open-label multicentre phase I/II trial evaluating the safety and efficacy of postnatal or prenatal and postnatal administration of allogeneic expanded fetal mesenchymal stem cells for the treatment of severe osteogenesis imperfecta in infants and fetuses: the BOOSTB4 trial protocol. *BMJ Open.* **14**, e079767 (2024).
16. Chan, J. et al. Stakeholder views and attitudes towards prenatal and postnatal transplantation of fetal mesenchymal stem cells to treat Osteogenesis Imperfecta. *Eur. J. Hum. Genet.* **27**, 1244–1253 (2019).
17. Moschidou, D. et al. Molecular signature of human amniotic fluid stem cells during fetal development. *Curr. Stem Cell. Res. Ther.* **8**, 73–81 (2013).
18. Hawkins, K. E. et al. Human Amniocytes Are Receptive to Chemically Induced Reprogramming to Pluripotency. *Mol. Ther.* **25**, 427–442 (2017).
19. Moschidou, D. et al. Valproic Acid Confers Functional Pluripotency to Human Amniotic Fluid Stem Cells in a Transgene-free Approach. *Mol. Ther.* **20**, 1953–1967 (2012).
20. Moschidou, D. et al. Human mid-trimester amniotic fluid stem cells cultured under embryonic stem cell conditions with valproic acid acquire pluripotent characteristics. *Stem Cells Dev.* **22**, 444–458 (2013).
21. Peister, A., Deutsch, E. R., Kolambkar, Y., Hutmacher, D. W. & Guldberg, R. E. Amniotic Fluid Stem Cells Produce Robust Mineral Deposits on Biodegradable Scaffolds. *Tissue Eng. Part. A*. **15**, 3129–3138 (2009).
22. Sun, H. et al. Osteogenic differentiation of human amniotic fluid-derived stem cells induced by bone morphogenetic protein-7 and enhanced by nanofibrous scaffolds. *Biomaterials* **31**, 1133–1139 (2010).

23. Trapani, M. D. et al. Immune regulatory properties of CD117(pos) amniotic fluid stem cells vary according to gestational age. *Stem Cells Dev.* **24**, 132–143 (2015).
24. Zare, E. et al. Replicative senescence in amniotic fluid-derived mesenchymal stem cells and its impact on their immunomodulatory properties. *Histochem. Cell. Biol.* **163**, 34 (2025).
25. Chen, Y. S. et al. Small molecule mesengenic induction of human induced pluripotent stem cells to generate mesenchymal stem/stromal cells. *Stem Cells Transl Med.* **1**, 83–95 (2012).
26. Wruck, W., Graffmann, N., Spitzhorn, L. S. & Adjaye, J. Human Induced Pluripotent Stem Cell-Derived Mesenchymal Stem Cells Acquire Rejuvenation and Reduced Heterogeneity. *Front. Cell. Dev. Biol.* **9**, 717772 (2021).
27. Jungbluth, P. et al. Human iPSC-derived iMSCs improve bone regeneration in mini-pigs. *Bone Res.* **7**, 32 (2019).
28. Spitzhorn, L. S. et al. Human iPSC-derived MSCs (iMSCs) from aged individuals acquire a rejuvenation signature. *Stem Cell. Res. Ther.* **10**, 100 (2019).
29. Moschidou, D. et al. Human mid-trimester amniotic fluid stem cells cultured under embryonic stem cell conditions with valproic acid acquire pluripotent characteristics. *Stem Cells Dev.* **22**, 444–458 (2013).
30. Hass, R., Kasper, C., Böhm, S. & Jacobs, R. Different populations and sources of human mesenchymal stem cells (MSC): A comparison of adult and neonatal tissue-derived MSC. *Cell. Commun. Signal.* **9**, 12 (2011).
31. Dominici, M. et al. Minimal criteria for defining multipotent mesenchymal stromal cells. The International Society for Cellular Therapy position statement. *Cytotherapy* **8**, 315–317 (2006).
32. Choudhery, M. S., Mahmood, R., Harris, D. T. & Ahmad, F. J. Minimum criteria for defining induced mesenchymal stem cells. *Cell. Biol. Int.* **46**, 986–989 (2022).
33. Brinkhof, B., Zhang, B., Cui, Z., Ye, H. & Wang, H. ALCAM (CD166) as a gene expression marker for human mesenchymal stromal cell characterisation. *Gene: X*. **5**, 100031 (2020).
34. Crisan, M., Corselli, M., Chen, W. C. & Péault, B. Moldovan, N. Perivascular cells for regenerative medicine. *J. Cell. Mol. Med.* **16**, 2851–2860 (2012).
35. Covas, D. T. et al. Multipotent mesenchymal stromal cells obtained from diverse human tissues share functional properties and gene-expression profile with CD146 + perivascular cells and fibroblasts. *Exp. Hematol.* **36**, 642–654 (2008).
36. Zhu, H. et al. The Role of the Hyaluronan Receptor CD44 in Mesenchymal Stem Cell Migration in the Extracellular Matrix. *STEM CELLS*. **24**, 928–935 (2006).
37. Veevers-Lowe, J., Ball, S. G., Shuttleworth, A. & Kielty, C. M. Mesenchymal stem cell migration is regulated by fibronectin through α5β1-integrin-mediated activation of PDGFR-β and potentiation of growth factor signals. *J. Cell. Sci.* **124**, 1288–1300 (2011).
38. Frith, J. E., Mills, R. J., Hudson, J. E. & Cooper-White, J. J. Tailored Integrin–Extracellular Matrix Interactions to Direct Human Mesenchymal Stem Cell Differentiation. *Stem Cells Dev.* **21**, 2442–

2456 (2012).

39. von Lersner, A., Droesen, L. & Zijlstra, A. Modulation of cell adhesion and migration through regulation of the immunoglobulin superfamily member ALCAM/CD166. *Clin. Exp. Metastasis*. **36**, 87–95 (2019).
40. Yang, E., Shim, J. S., Woo, H. J., Kim, K. W. & Kwon, H. J. Aminopeptidase N/CD13 induces angiogenesis through interaction with a pro-angiogenic protein, galectin-3. *Biochem. Biophys. Res. Commun.* **363**, 336–341 (2007).
41. Ries, C. et al. MMP-2, MT1-MMP, and TIMP-2 are essential for the invasive capacity of human mesenchymal stem cells: differential regulation by inflammatory cytokines. *Blood* **109**, 4055–4063 (2007).
42. Kundu, A. K., Khatiwala, C. B. & Putnam, A. J. Extracellular Matrix Remodeling, Integrin Expression, and Downstream Signaling Pathways Influence the Osteogenic Differentiation of Mesenchymal Stem Cells on Poly(Lactide-Co-Glycolide) Substrates. *Tissue Eng. Part. A*. **15**, 273–283 (2009).
43. Burk, J., Sassmann, A., Kasper, C., Nimptsch, A. & Schubert, S. Extracellular Matrix Synthesis and Remodeling by Mesenchymal Stromal Cells Is Context-Sensitive. *Int. J. Mol. Sci.* **23**, 1758 (2022).
44. Maacha, S. et al. Paracrine Mechanisms of Mesenchymal Stromal Cells in Angiogenesis. *Stem Cells Int.* 4356359 (2020). (2020).
45. Tao, H., Han, Z., Han, Z. C. & Li, Z. Proangiogenic Features of Mesenchymal Stem Cells and Their Therapeutic Applications. *Stem Cells Int.* 1314709 (2016). (2016).
46. Song, H., Yin, D. & Liu, Z. GDF-15 promotes angiogenesis through modulating p53/HIF-1α signaling pathway in hypoxic human umbilical vein endothelial cells. *Mol. Biol. Rep.* **39**, 4017–4022 (2012).
47. Cheng, Y., Gu, W., Zhang, G. & Guo, X. Notch1 activation of Jagged1 contributes to differentiation of mesenchymal stem cells into endothelial cells under cigarette smoke extract exposure. *BMC Pulm Med.* **22**, 139 (2022).
48. Sun, J. et al. Notch ligand Jagged1 promotes mesenchymal stromal cell-based cartilage repair. *Exp. Mol. Med.* **50**, 1–10 (2018).
49. Grafe, I. et al. TGF-β Family Signaling in Mesenchymal Differentiation. *Cold Spring Harb Perspect. Biol.* **10**, a022202 (2018).
50. Zhang, P. et al. Histone H3K9 Acetyltransferase PCAF Is Essential for Osteogenic Differentiation Through Bone Morphogenetic Protein Signaling and May Be Involved in Osteoporosis. *STEM CELLS*. **34**, 2332–2341 (2016).
51. Tontanahal, A., Arvidsson, I. & Karpman, D. Annexin Induces Cellular Uptake of Extracellular Vesicles and Delays Disease in Escherichia coli O157:H7 Infection. *Microorganisms* **9**, 1143 (2021).
52. Kinoshita, T. Biosynthesis and biology of mammalian GPI-anchored proteins. *Open. Biol.* **10**, 190290 (2020).
53. Aula, N., Kopra, O., Jalanko, A. & Peltonen, L. Sialin expression in the CNS implicates extralysosomal function in neurons. *Neurobiol. Dis.* **15**, 251–261 (2004).

54. Martin, K. R., Wong, H. L., Witko-Sarsat, V. & Wicks, I. P. G-CSF – A double edge sword in neutrophil mediated immunity. *Semin Immunol.* **54**, 101516 (2021).
55. Kent, D. et al. Regulation of Hematopoietic Stem Cells by the Steel Factor/KIT Signaling Pathway. *Clin. Cancer Res.* **14**, 1926–1930 (2008).
56. Scott, M. A., Nguyen, V. T., Levi, B. & James, A. W. Current Methods of Adipogenic Differentiation of Mesenchymal Stem Cells. *Stem Cells Dev.* **20**, 1793–1804 (2011).
57. Pollak, M. Insulin and insulin-like growth factor signalling in neoplasia. *Nat. Rev. Cancer*. **8**, 915–928 (2008).
58. Jin, X., Tian, S. & Li, P. Histone Acetyltransferase 1 Promotes Cell Proliferation and Induces Cisplatin Resistance in Hepatocellular Carcinoma. *Oncol. Res. Featur Preclin Clin. Cancer Ther.* **25**, 939–946 (2017).
59. Capone, V. et al. HAT1: Landscape of Biological Function and Role in Cancer. *Cells* **12**, 1075 (2023).
60. Komori, T. Regulation of bone development and extracellular matrix protein genes by RUNX2. *Cell. Tissue Res.* **339**, 189 (2009).
61. Vimalraj, S., Arumugam, B., Miranda, P. J. & Selvamurugan, N. Runx2: Structure, function, and phosphorylation in osteoblast differentiation. *Int. J. Biol. Macromol.* **78**, 202–208 (2015).
62. Modica, S. & Wolfrum, C. The dual role of BMP4 in adipogenesis and metabolism. *Adipocyte* **6**, 141–146 (2017).
63. Kim, H. J. & Im, G. I. Electroporation-Mediated Transfer of SOX Trio Genes (SOX-5, SOX-6, and SOX-9) to Enhance the Chondrogenesis of Mesenchymal Stem Cells. *Stem Cells Dev.* **20**, 2103–2114 (2011).
64. Coleman, C. M. et al. Growth Differentiation Factor-5 Enhances In Vitro Mesenchymal Stromal Cell Chondrogenesis and Hypertrophy. *Stem Cells Dev.* **22**, 1968–1976 (2013).
65. Zhao, M. et al. Smurf1 Inhibits Osteoblast Differentiation and Bone Formation in Vitro and in Vivo *. *J. Biol. Chem.* **279**, 12854–12859 (2004).

Figures

Figure 1

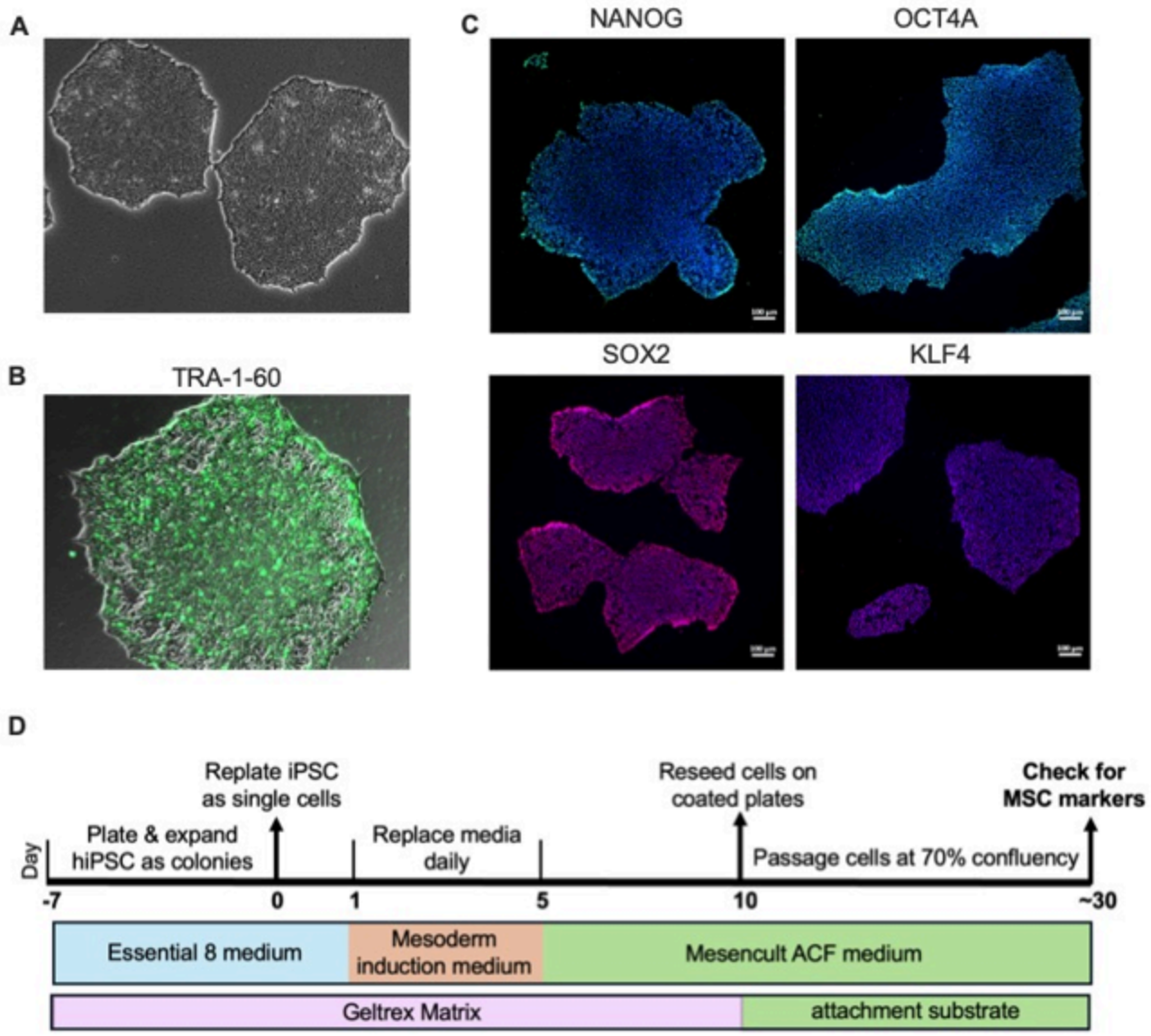


Figure 1

Characterisation of hiPSCs and directed differentiation into iMSCs. A. Phase-contrast image showing hiPSCs growing as compact colonies with typical pluripotent stem cell morphology. Original magnification, ×40. **B.** Live immunofluorescence staining showing expression of the pluripotency-associated surface marker TRA-1-60 in hiPSCs (green). Original magnification, ×40. **C.** Immunofluorescence analysis showing expression of the pluripotency-associated markers NANOG, OCT4A, SOX2 and KLF4 in hiPSC colonies. Nuclei were counterstained with DAPI (blue). Scale bars, 100 µm. **D.** Schematic representation of the protocol used to differentiate hiPSCs into iMSCs, including

expansion of hiPSC colonies, single-cell replating, mesoderm induction, culture in MesenCult ACF medium, substrate transition and assessment of MSC marker expression at approximately day 30.

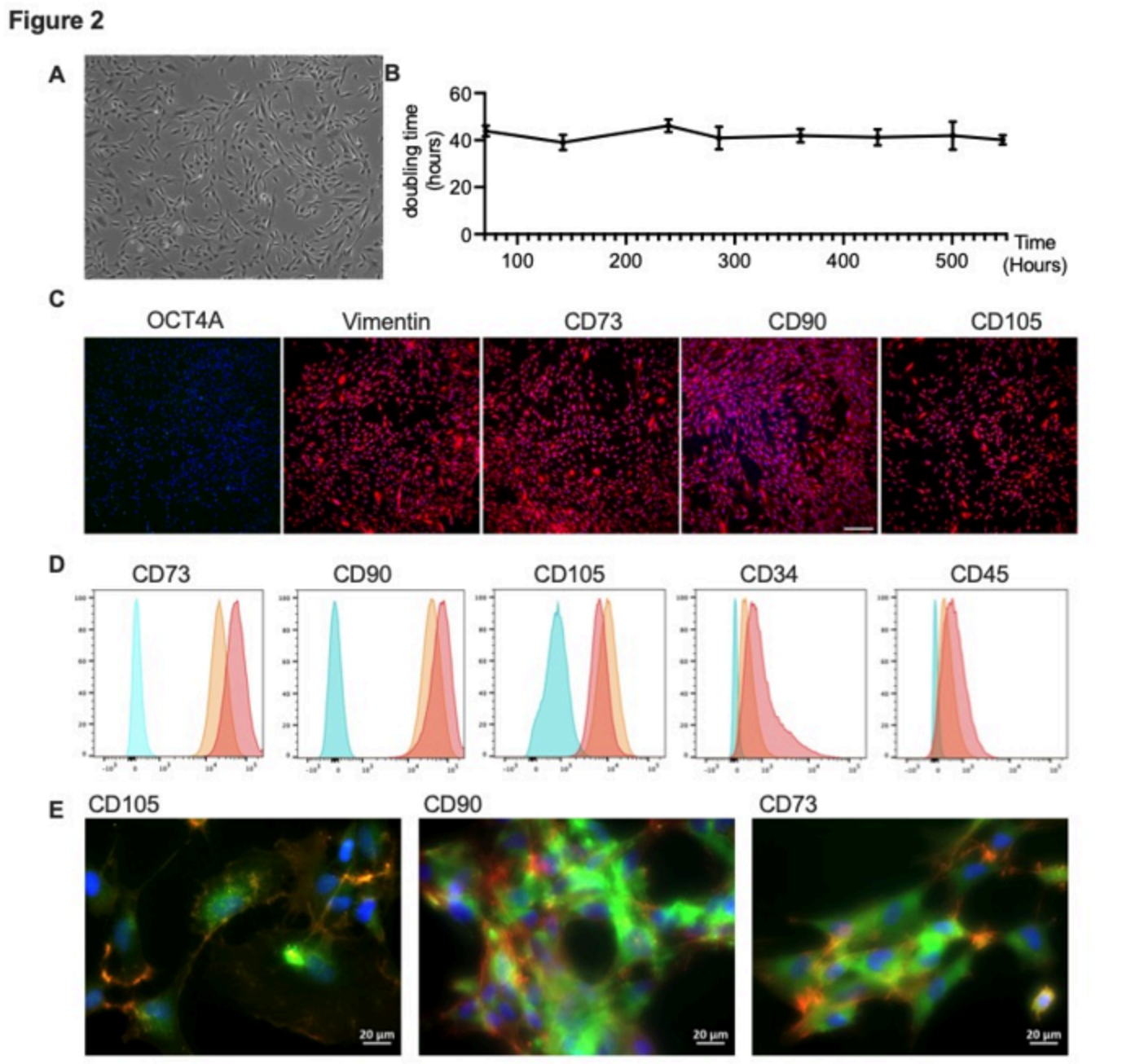


Figure 2

Characterisation of iMSCs. A. Phase-contrast image showing AF-iMSCs displaying an adherent, spindle-shaped, fibroblast-like morphology. Original magnification, ×40. **B.** Growth-kinetic analysis of AF-iMSCs cultured in expansion medium over approximately 600 h, showing population-doubling time over time. Data are presented as mean ± SEM. **C.** Immunofluorescence analysis showing absence of detectable OCT4A expression and expression of the mesenchymal-associated markers vimentin, CD73, CD90 and

CD105 in AF-iMSCs. Nuclei were counterstained with DAPI (blue). Original magnification, ×40. **D.** Flow-cytometry analysis of CD73, CD90, CD105, CD34 and CD45 expression. Red histograms represent stained AF-iMSCs, orange histograms represent stained parental AFSCs, and blue histograms represent unstained AF-iMSCs used as negative controls. **E.** Immunofluorescence analysis showing expression of the MSC-associated markers CD105, CD90 and CD73 in AF-iMSCs. Nuclei were counterstained with DAPI (blue), and F-actin was counterstained with phalloidin (red). Scale bars, 20 μm.

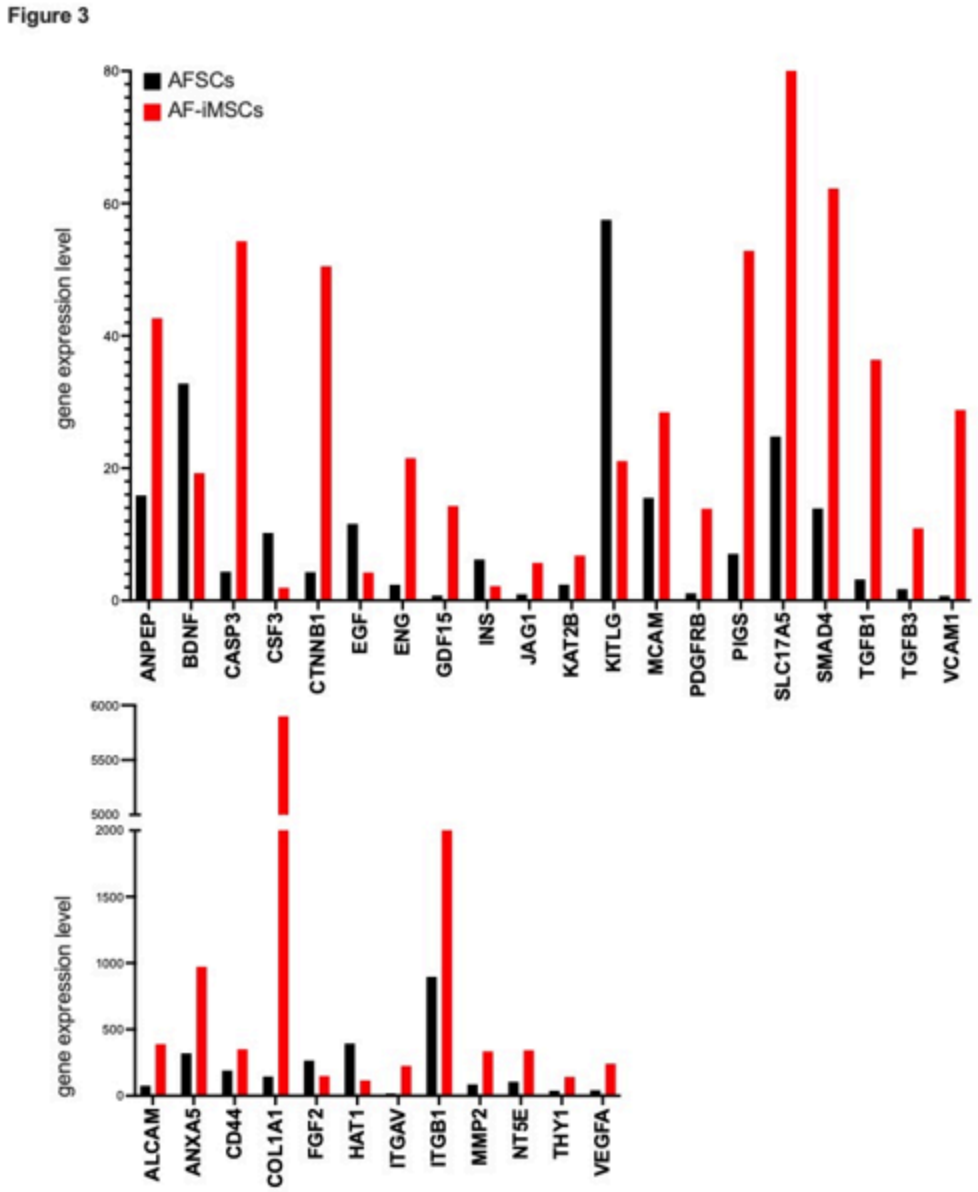


Figure 3

Comparative gene-expression profiling of AF-iMSCs and primary AFSC. Gene expression analysis of AF-iMSCs and primary human amniotic fluid stem cells (AFSCs) was performed using the RT² Profiler PCR Array for human mesenchymal stem cell-associated genes (PAHS-082Z). Gene-expression levels are shown for AF-iMSCs (red bars) and AFSCs (black bars) and are expressed as 2^-ΔCt values relative

to the housekeeping genes GAPDH, ACTB, B2M and HPRT1. The upper and lower graphs show genes plotted on different y-axis scales to accommodate differences in expression range.

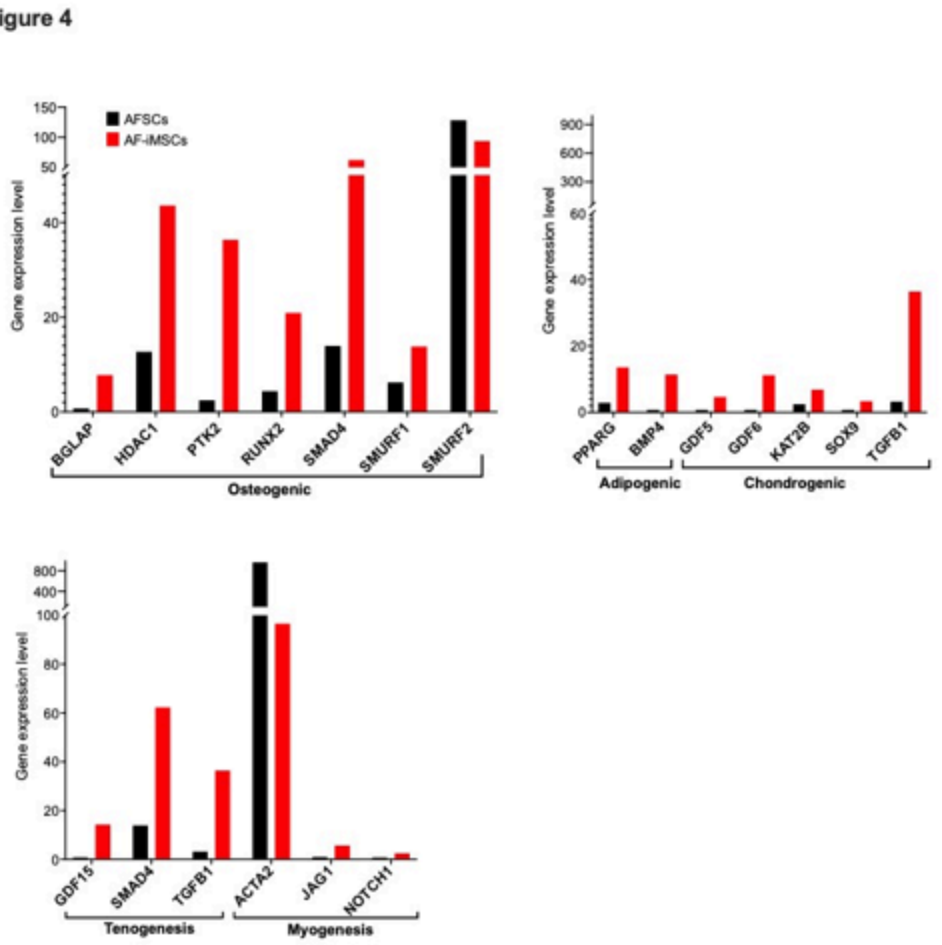


Figure 4

Comparative expression of lineage-associated genes in AF-iMSCs and primary AFSC. Gene expression analysis of AF-iMSCs and primary human amniotic fluid stem cells (AFSCs) was performed using the RT² Profiler PCR Array for human mesenchymal stem cell-associated genes (PAHS-082Z). Gene-expression levels are shown for AF-iMSCs (red bars) and AFSCs (black bars) and are expressed as 2^-ΔCt values relative to the housekeeping genes GAPDH, ACTB, B2M and HPRT1. Genes are grouped according to their association with osteogenic, adipogenic, chondrogenic, tenogenic and myogenic lineage programmes. Broken y-axes indicate genes with substantially higher expression levels.

Figure 5

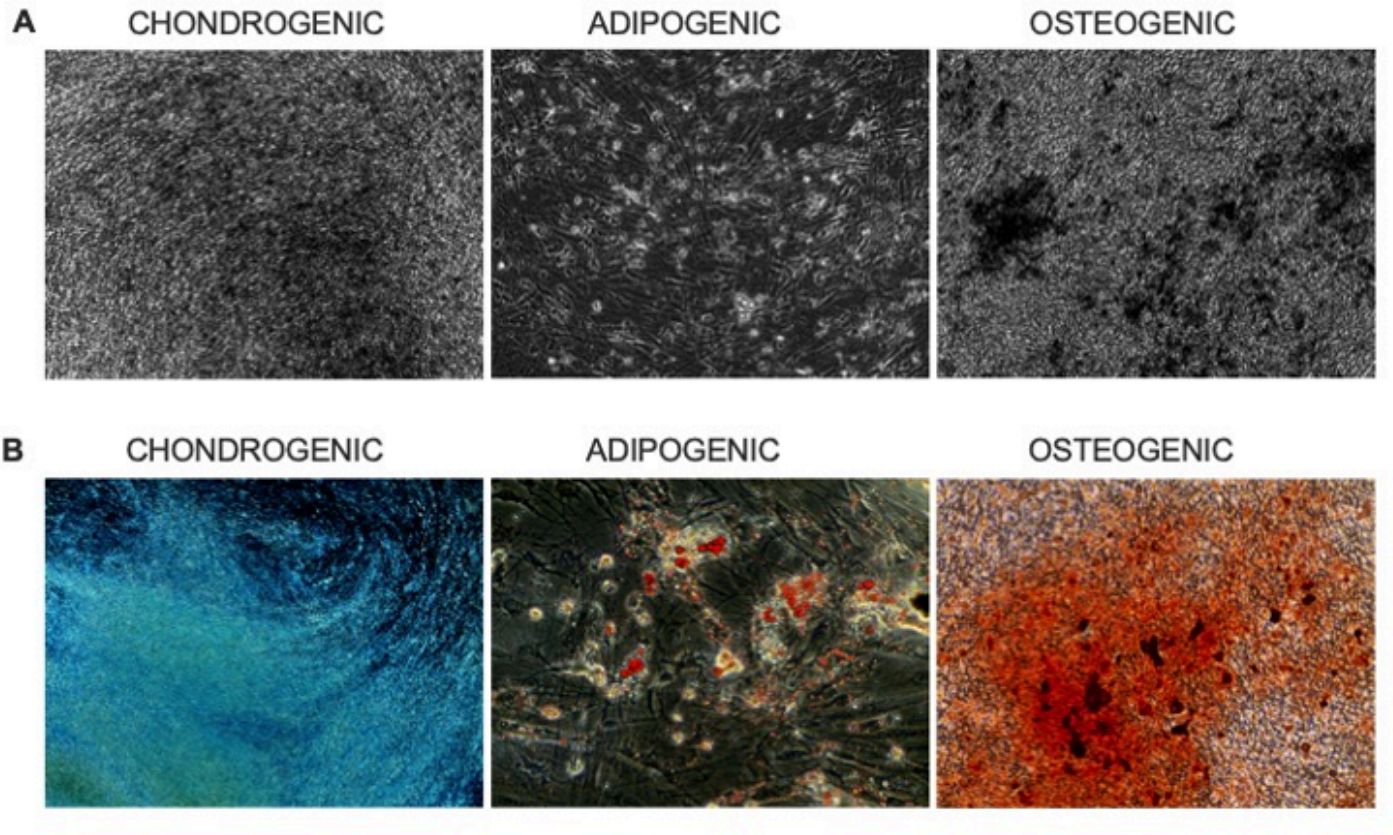


Figure 5

Trilineage differentiation potential of AF-iMSCs. A. Representative phase-contrast images of AF-iMSCs cultured under chondrogenic, adipogenic and osteogenic induction conditions for 21, 14 and 21 days, respectively. Original magnification, ×20. **B.**Lineage-specific staining confirming multilineage differentiation potential. Chondrogenic differentiation was assessed by Alcian Blue staining of glycosaminoglycan-rich extracellular matrix, adipogenic differentiation by Oil Red O staining of intracellular lipid droplets, and osteogenic differentiation by Alizarin Red staining of mineralised matrix deposition. Original magnification, ×20.

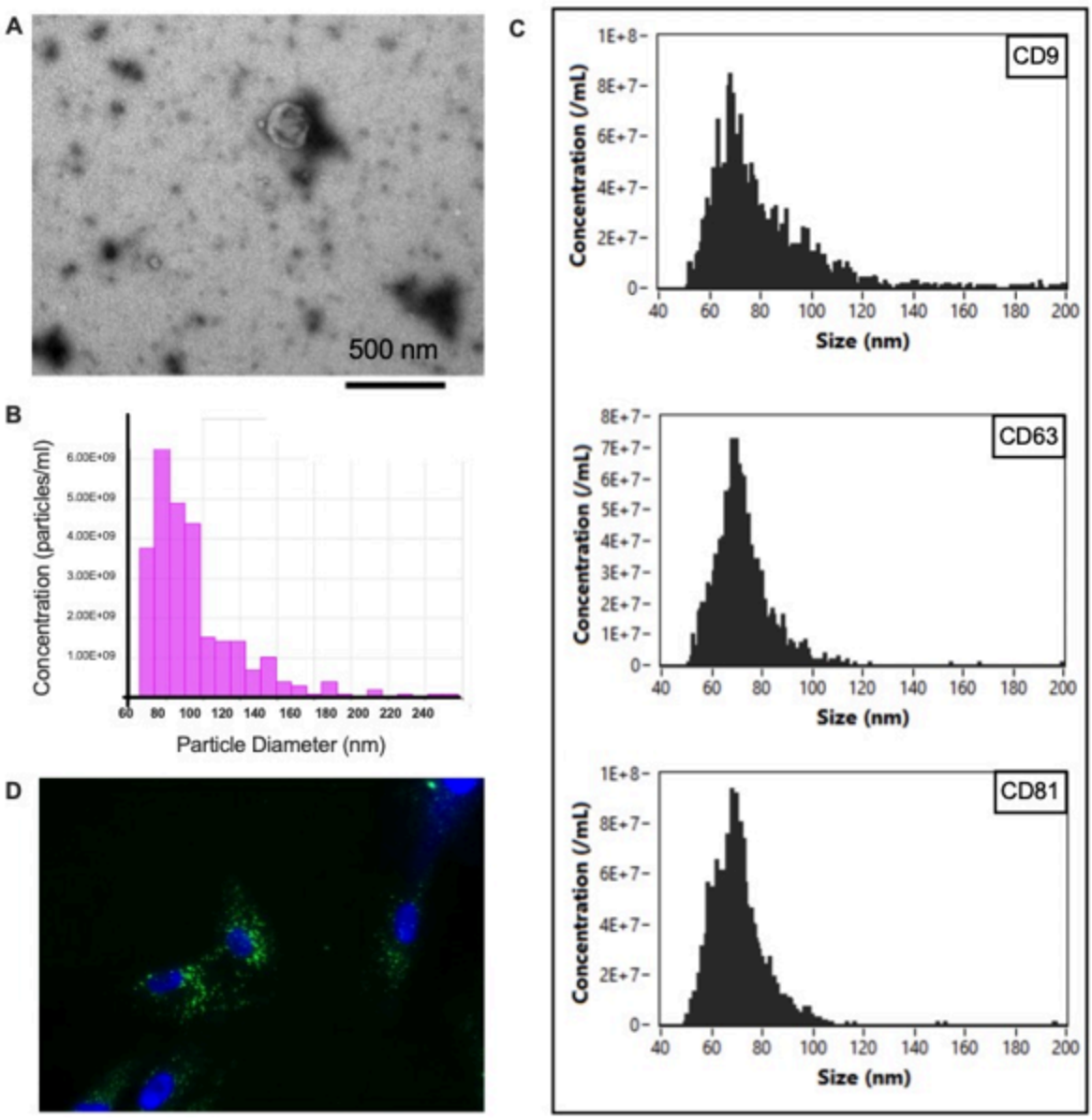


Figure 6

Characterisation of extracellular vesicles secreted by AF-iMSCs. A. Transmission electron microscopy (TEM) image of AF-iMSC-derived extracellular vesicles (iEVs), showing membrane-bound vesicles with a round to cup-shaped morphology. Scale bar, 500 nm. **B.** Particle concentration and size distribution of iEVs assessed by tunable resistive pulse sensing (TRPS; IZON). **C.**Nano-flow cytometry analysis of iEVs positive for EV-associated tetraspanins CD9, CD63 and CD81, showing particle concentration and size distribution for each marker-positive population. **D.**Representative fluorescence image showing uptake of BioTracker 655 red-labelled iEVs by human fibroblasts. Nuclei were counterstained with DAPI (blue). Original magnification, ×40.

Figure 7

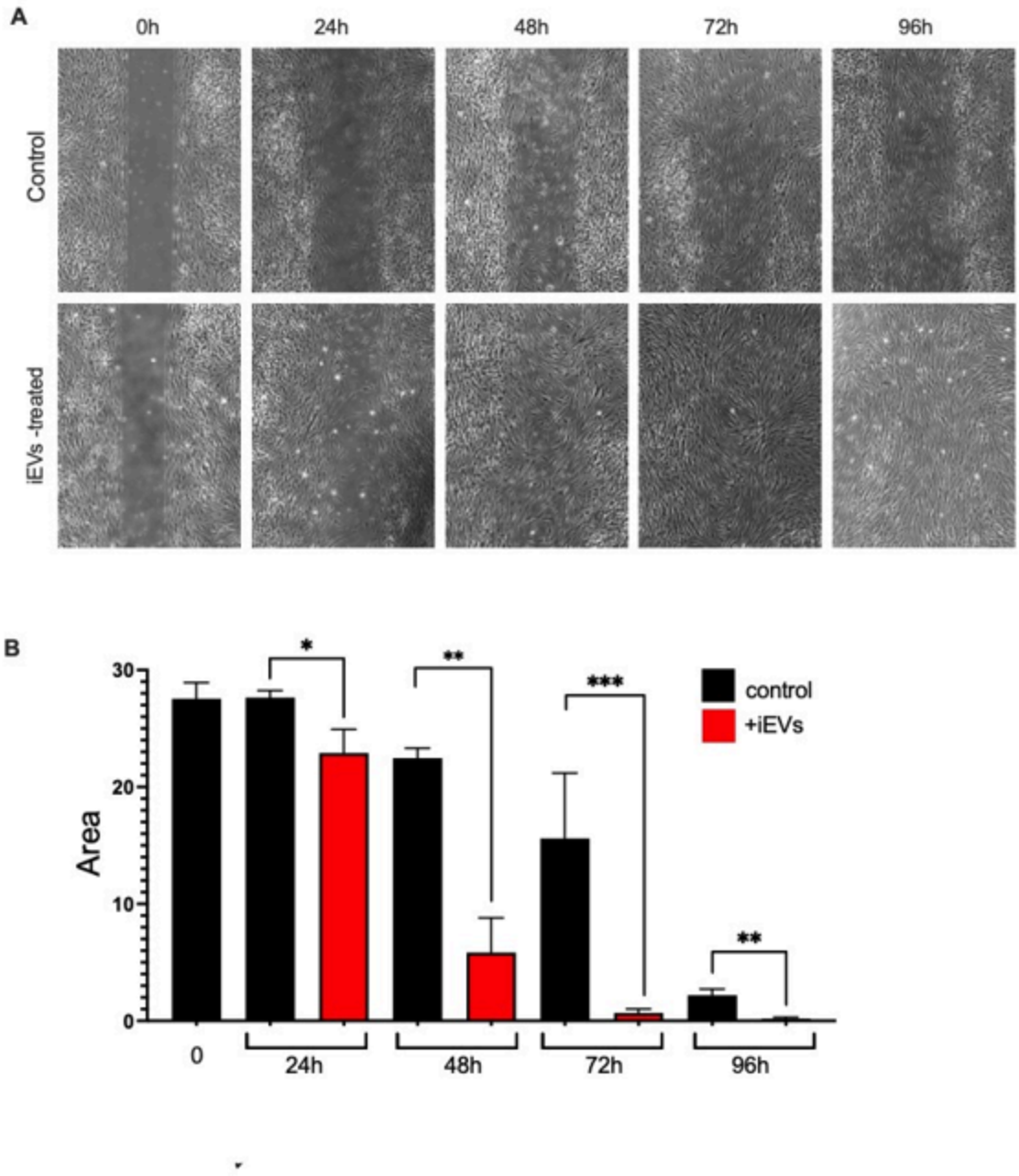


Figure 7

AF-iMSC-derived iEVs promote human fibroblast migration in vitro. A. Representative phase-contrast images of human fibroblast cultures immediately after generation of a cell-free gap using an ibidi culture insert (0 h), and after 24, 48, 72 and 96 h in the absence (control) or presence of AF-iMSC-derived iEVs (10^8 iEVs/ml). Original magnification, ×5. **B.** Quantification of the remaining cell-free area over time using Fiji/ImageJ. The WHPlugin measures the fraction of the total area covered by wound (Percent wound area). Data are presented as mean ± SD, n = 3. *P < 0.05, **P < 0.01, ***P < 0.001.

Figure 8

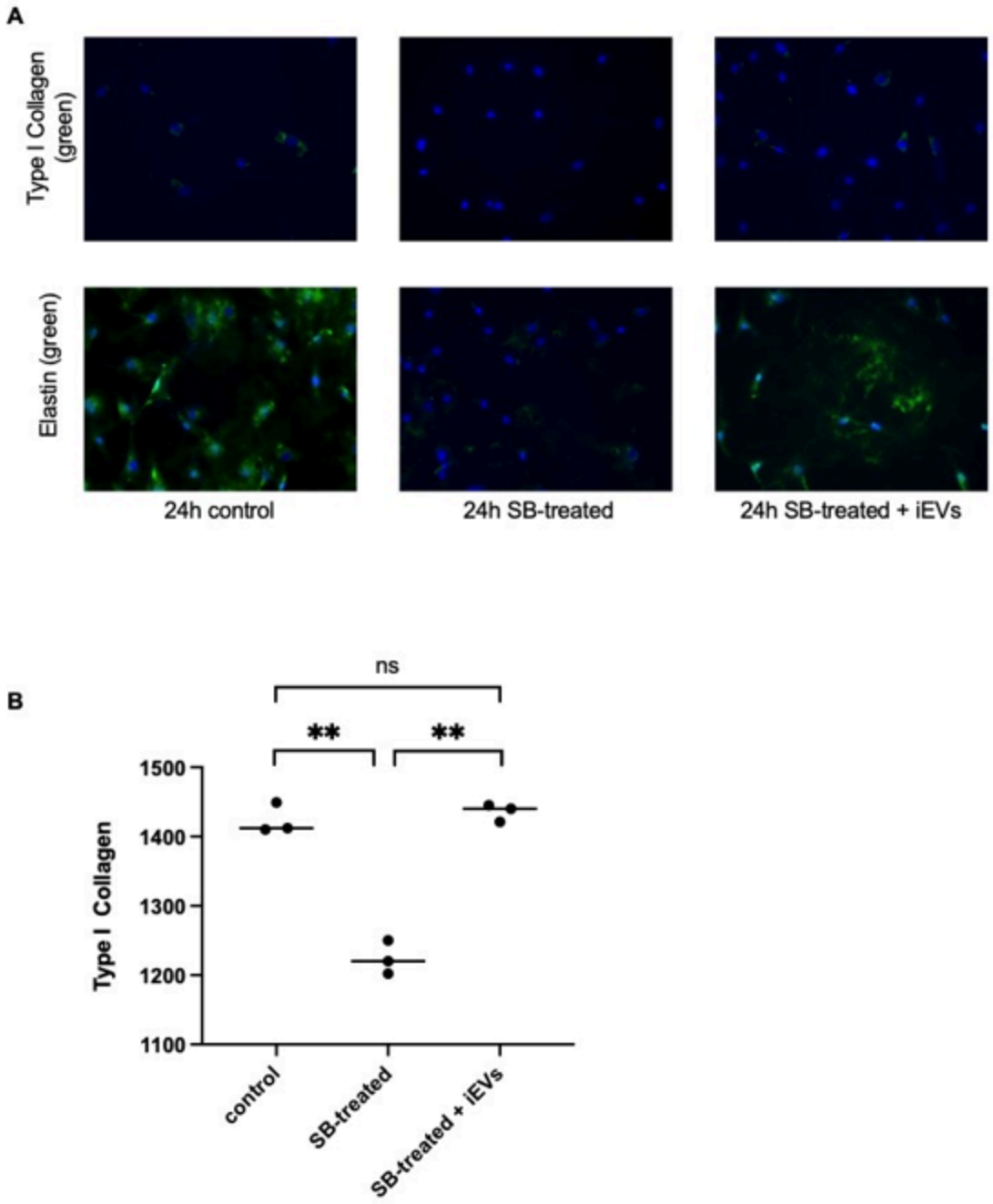


Figure 8

Potential of iEVs to stimulate human fibroblast migration in vitro. A. Representative immunofluorescence images of human fibroblasts cultured for 24 h under control conditions, in the presence of the TGF-β receptor inhibitor SB431542 (SB), or in the presence of SB431542 with AF-iMSC-derived iEVs. Type I collagen and elastin are shown in green, and nuclei were counterstained with DAPI (blue). Original magnification: ×40. **B.** ELISA quantification of type I collagen in fibroblast culture supernatants under control, SB-treated and SB + iEV-treated conditions. Data are presented as individual values with mean, n = 3. **P < 0.01; ns, not significant.